BEN-GURION UNIVERSITY OF THE NEGEV
FACULTY OF ENGINEERING SCIENCES
DEPARTMENT OF BIOMEDICAL ENGINEERING

Entropy-driven aggregation of adhesion sites of supported membranes

Thesis submitted in partial fulfillment of the requirements for the $M.S_c$ degree

By: Noam Weil

September, 2011

September, 2011

BEN-GURION UNIVERSITY OF THE NEGEV

FACULTY OF ENGINEERING SCIENCES

DEPARTMENT OF BIOMEDICAL ENGINEERING

Entropy-driven aggregation of adhesion sites of supported membranes

Thesis submitted in partial fulfillment of the requirements for the M.S$_c$ degree

By: Noam Weil

Supervised by: Dr. Oded Farago

Author:..... Date:.....

Supervisor:..... Date:.....

Chairman of Graduate Studies Committee:.....Date:.....

September, 2011

Abstract

Adhesion bonds between membranes and surfaces are attracted to each other via effective interactions whose origin the entropy loss due to the reduction in the amplitude of the membrane thermal fluctuations in the vicinity of the adhesion bonds. However, these interactions have non-trivial many-body characteristics which, in addition to the steric repulsion between the fluctuating membrane and the surface, create a difficulty to analyze the adhesion bonds distribution. In this thesis, we use mean-field calculations and Monte Carlo simulations, and analyze this problem. We show that while the fluctuation-mediated interactions alone are not sufficient to allow the formation of aggregation domains, they greatly reduce the strength of the direct interactions required to facilitate cluster formation. In addition, the fluctuation-induced interactions are also expected to drive the adhesion bonds towards the rim of a cell, as well as towards the surfaces of membrane inclusions. We analyze the attraction of adhesion bonds to the cell inner and outer boundaries. Our analysis shows that the probability distribution function of a single (diffusing) adhesion bond decay algebraically with the distance from the boundaries. Upon increasing the concentration of the adhesion bonds, the attraction to the boundaries becomes strongly self-screened.

Acknowledgments

I wish to thank my supervisor, Dr. Oded Farago, for all the support, encouragement, guidance, and constructive criticism from the beginning of my project until the final stages of my research work.

Special thanks to my friends and lab colleagues: Nadiv Dharan, Yotam Y. Avital and Mor Ben Tov, for their illuminating assistance, and fruitful conversations during the past two years.

Finally, thanks to all others, whom I did not mention here, that helped in many other ways to make this work possible.

Contents

Chapter 1

Introduction

1.1 Biological and supported membranes

Fatty acids and other lipids, due to their amphiphilic nature, are spontaneously self-assemble into bilayer membranes that define the limits of cells and serve as permeability barrier to prevent proteins, ions and metabolites from leaking out of the cell and unwanted toxins leaking in [1]. In eukaryotic cells, membranes also surround the organelles allowing for organization of biological processes through compartmentalization. In addition, biological membranes host numerous proteins (shown schematically in fig. 1.1) that are crucial for the mechanical stability of the cell, and which carry out a variety of functions such as energy and signal transduction, communication, and cellular homeostasis [2]. Most biological membranes are found in the fluid phase where the lipids comprising the bilayer can diffuse freely in the membrane plane. Another characteristic feature of lipid bilayers is their high flexibility which allows for large thermally excited undulations [1, 3]. The fluidity and low rigidity of membranes are important for many of their biological properties, such as their ability to change their shape easily and the possibility of proteins to insert themselves into the membrane [4].

An important aspect of biological membranes is that they are typically not free but

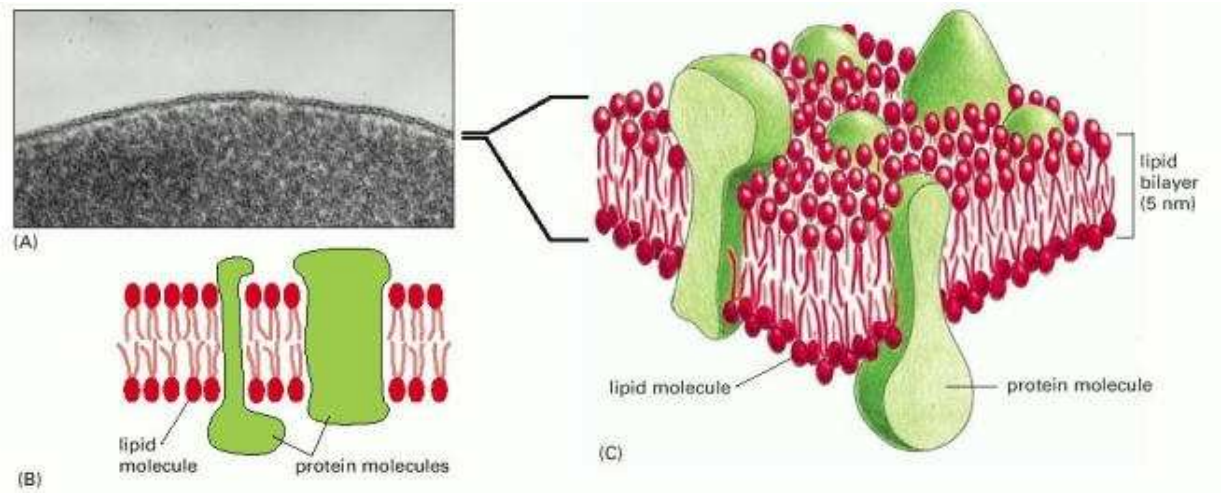

Figure 1.1: (A) An electron micrograph of a plasma membrane (of a human red blood cell) seen in cross-section. (B) and (C) are schematic drawings showing, respectively, two and three-dimensional view of a cell membrane. (Adapted from [2])

rather confined by other surrounding membranes, adhere to other membranes, and attach to elastic networks like the cytoskeleton and the extracellular matrix. Several model systems with reduced compositional complexity have been designed to mimic biological membranes. These biomimetic systems include phospholipid bilayers deposited onto solid substrates (solid-supported membranes) [5], or on ultra-thin polymer supports (polymer-supported membranes) [6]. Placing a membrane on a flat substrate allows for the application of several different surface sensitive techniques, including atomic force microscopy, x-ray and neutron diffraction, ellipsometry, nuclear magnetic resonance, and others [7]. With the aid of biochemical tools and generic engineering, supported membranes can be functionalized with various membrane-associated proteins [8]. Synthetic supported membranes with reconstituted proteins are increasingly used as controlled idealized models for studying key properties of cellular membranes [9]. They provide a natural environment for the immobilization of proteins under nondenaturating conditions and in well defined orientations [10]. Another attractive application of supported membranes is the design of phantom cells exhibiting well defined adhesive properties and receptor densities [11]. Using advanced imaging techniques, detailed information can be obtained about the structure of the adhesion zone between the

receptor-functionalized supported membrane and ligand-containing vesicles that can bind to the supported membrane [12,13]. These studies provide insight into the dynamics of adhesion processes and the molecular interactions involved in cell adhesion [14, 15]. Understanding these interactions is crucial for the development of drug delivery systems that depend on efficient adhesion between a liposome and the plasma membrane of the target cell.

1.2 Theoretical models for membranes

1.2.1 Modeling membranes on multiple scales

In order to study the physical properties of cell adhesion in particular and membrane processes in general, several models have been used to describe these system. The models divers by their time and length scales representation, where they roughly divide into atomistic, coarse-grained, and elasticity models (Illustrate in fig. 1.2). Atomistic models describe bilayer membrane properties with chemical accuracy. Molecular architecture and interactions are faithfully modeled including electrostatic interactions, torsional, and bending potentials. Atomistic models are used to examine membrane patches of a few nanometers over time scales of a few tens of nanoseconds [16]. On the other hand, the elasticity model (see next sect. 1.2.2) refer to membrane as an infinitely thin, elastic sheet, of a macroscopic scale which characterized by a surface tension, spontaneous curvature, and bending rigidity. Although these models can address large length scales, they have difficulty describing the processes that evolve on the scale of the membrane thickness itself and cannot describe those that involve changes in lipid conformations [17].

Coarse-grained models represent a mid-state between the atomistic and the elasticity models. In these models the structure of the amphiphilic, proteins and water molecules is represented in a "coarse-grained" manner where a number of atoms are grouped together into a single site [18]. Coarse-grained models can be studied by a variety of techniques including Monte Carlo (MC) simulation, molecular dynamics, dissipative particle dynamics [18–21],

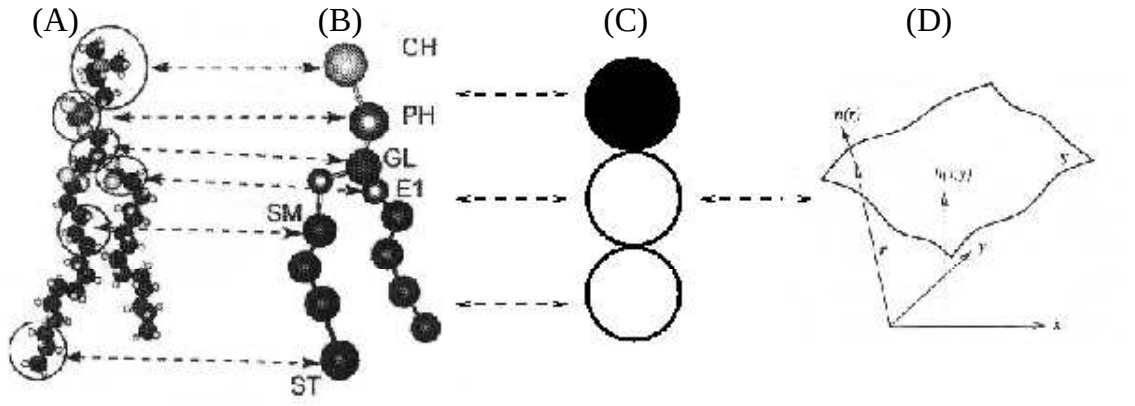

Figure 1.2: Illustration of the various models of a membrane: starting from the atomistic model (A), through different levels of coarse-grained models (B and C) and ends with the elasticity model(D).

dynamical density functional theory [22], and self-consistent field theory [23]. The coarse-grained approach simplifies computer simulations of membranes and significantly reduces their running time. The reduction becoming even larger when using a "water-free" coarse-grained computed simulations (simplified models where instead of water molecules, there is a hydrophobic-like potential between the amphiphilic molecules tails) [18, 24–26]. In addition, for high number of molecules grouped together, the length and time scale of the coarse-grained model and the elasticity model can overlap. This allows the comparison between elastic continuum theoretical models of membranes such as Ginzburg-Landau free energy functionals [27] or the effective surface Hamiltonian [1, 3, 27, 28], with "coarse-grained", discrete computed simulations results.

1.2.2 Helfrich effective Hamiltonian

On a macroscopic length scale, the molecular architecture of a bilayer membrane is negligible. Therefore, one can implement the elasticity model and consider the bilayer membrane as a smooth continuous sheet that fluctuates. The thermal fluctuations can be studied with

Helfrich Hamiltonian [28] relating the elastic energy to the shape of the membrane,

$$\mathcal{H} = \int_S dA \left[\sigma + \frac{1}{2}\kappa(c_1 + c_2 - 2c_0)^2 + \kappa_G c_1 c_2 \right]. \tag{1.1}$$

The integration in the above equation is carried over the whole surface of the membrane. Three elastic moduli are involved with the Helfrich Hamiltonian: the surface tension σ, the bending modulus κ and the saddle-splay modulus κ_G. The quantities c_1 and c_2 appearing in the above equation are the local principle curvatures of the surface and c_0 is the spontaneous curvature of the surface (for a flat bilayers $c_0 = 0$). If one only considers fluctuations which do not change the topology of the membrane, then the total energy associated with the last term in eq. 1.1 is a constant [28]. A way to parameterize a fluctuating flat membrane, is to use the Monge representation, where the surface is represented by a height function, $z = h(x, y)$, above a reference $x - y$ plane [29]. Thus, eq. 1.1 (without its last term and for $c_0 = 0$) is simplified to the following approximation

$$\mathcal{H} = \int d^2\vec{r} \left[\frac{1}{2}\sigma(\vec{\nabla}h)^2 + \frac{1}{2}\kappa(\nabla^2 h)^2 \right]. \tag{1.2}$$

Note that in addition to the bending energy and surface tension, other energy contributions can be added to the Helfrich Hamiltonian such as harmonic confining potential.

For a freely fluctuating membrane, the discrete Helfrich Hamiltonian is most conveniently handled in Fourier space where the height function is represented by a set of independent oscillating modes $\vec{q}$

$$h(\vec{r}) = \frac{1}{L}\sum_{\vec{q}} h_{\vec{q}} \exp\left(i\vec{q}\vec{r}\right), \tag{1.3}$$

where L is the linear length of the membrane. In Fourier space, the different modes decouple

into independent harmonic oscillators, and the Hamiltonian (1.2) read

$$\mathcal{H} = \frac{l^4}{L^2} \sum_{\vec{q}} \left[\frac{\kappa}{2} |\vec{q}|^4 + \frac{\sigma}{2} |\vec{q}|^2 \right] |h_{\vec{q}}|^2, \tag{1.4}$$

where l is of the order of the bilayer membrane thickness. By invoking the equipartition theorem, one can easy to derive that the mean squared amplitude of the Fourier modes of $h(\vec{r})$ is equal to

$$\langle |h_q|^2 \rangle = \frac{k_B T L^2}{l^4(\kappa q^4 + \sigma q^2)}, \tag{1.5}$$

where k_B is the Boltzmann factor, T is the temperature, and q is the wave vector size.

1.3 Adhesion fluctuation-induced interactions

1.3.1 The cell adhesion process

Supported membranes create an appropriate platform for the investigation and the observation of cell adhesion. This process, during which the cell membrane is attracted to another interface (which may be the membrane of another cell), can, in principle, be facilitated by non-specific attractive interactions (e.g., Coulomb and van der Waals interactions). Most often, however, cell adhesion is mediated by specific binding between receptors that reside on the membrane surface and ligands located on the opposite surface [30]. Specific adhesion usually occurs in regions with high density of receptors and ligands. When facing a surface with enough ligands, the receptors may cluster into highly concentrated adhesion domains to establish strong binding [31, 32]. Specific bioadhesion occurs in a variety of cellular processes, including binding of white blood cells to pathogens [33], binding and fusion of drug carrier liposome to target cells [34], cadherin-mediated adhesion of neighboring cells [35], focal adhesion of cells to the extracellular matrix [36], and cell signaling. (See examples in

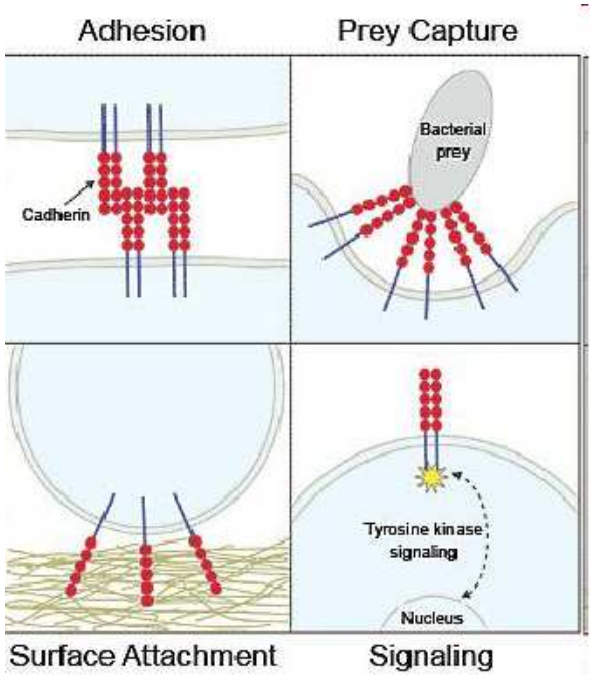

Figure 1.3: Biological examples of specific binding between receptors and ligands.

fig. 1.3)

Adhesion induced domain formation requires some attractive intermolecular interactions between the receptor-ligand pairs. These interactions include both direct and membrane-mediated contributions. The former are typically described by pairwise potentials which are infinitely repulsive at very small molecular separations and attractive at somewhat longer (but still finite) distances [37]. Their effect can, therefore, be studied in the framework of the thoroughly researched lattice-gas model [38]. In contrast, much less is known about the membrane-mediated mechanism, which has been proposed by Braun *et al.* to explain to formation of gap junctional plaque at cell-cell interfaces [39], and whose origin can be understood as follows: Consider two adhesion bonds between two membranes or between a membrane and a surface (fig. 1.4(A)). The adhesion bonds restrict the thermal height fluctuations of the membrane in their vicinity. This entropy loss can be minimized if the two adhesion bonds are brought to the same place (fig. 1.4(B)), in which case the membrane becomes pinned at only one place rather than two. The membrane fluctuations, thus, induce an attractive potential of mean force between the adhesion bonds.

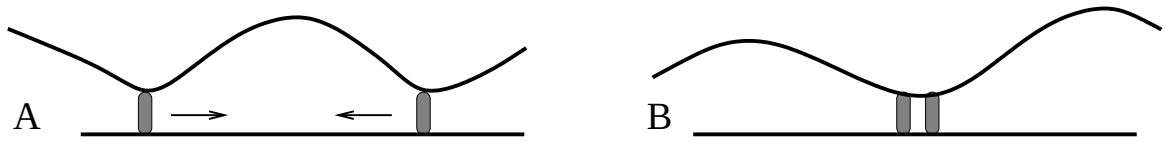

Figure 1.4: (A) Schematic of a membrane attached by two distant adhesion bonds to an underlying surface. There is an entropy penalty associated with each adhesion bonds due to the restrictions imposed on the membrane thermal fluctuations in their vicinity. (B) The entropy cost can be minimized by bringing the adhesion bonds close to each other, in which case the thermal fluctuations become limited at only one location. The increase in the entropy in (B) compared to (A) is the origin of the attractive fluctuation-induced interactions between the adhesion bonds. (Adapted from [40])

1.3.2 Statistical mechanics of a membrane with one and two adhesion bond

The problem of a membrane with one and two adhesion bonds was studied by Farago in [41] and [42], respectively. In the case of a single adhesion bond, we consider the system shown schematically in fig. 1.5, which consists of a tensionless membrane with a linear size L that fluctuates above a flat impenetrable surface and pinned to it at one fixed point located at r_0 ($h(r_0) = 0$). The elastic curvature energy of the membrane is given by the Helfrich effective Hamiltonian (see eq. 1.2 with $\sigma = 0$)

$$\mathcal{H} = \int \left[\frac{1}{2}\kappa(\nabla^2 h)^2\right] \Phi(h)\delta\left[h(\vec{r_0})\right] d^2\vec{r}. \tag{1.6}$$

In eq. 1.6, Φ represents represents the hard wall constraint due to the surface ($\Phi = 1$ for $h \geq 0$, and $\Phi = +\infty$ for $h < 0$), δ is the Dirac delta-function. Using statistical mechanical arguments, Farago has shown [41] that, the attachment free-energy cost, associated with the entropy loss, of a single adhesion bond is given by

$$F_1 = k_B T \ln\left(\frac{L^2}{l^2}\right) = 2k_B T \ln\left(\frac{L}{l}\right). \tag{1.7}$$

In addition, it has demonstrated that pinning the membrane to the surface at one point

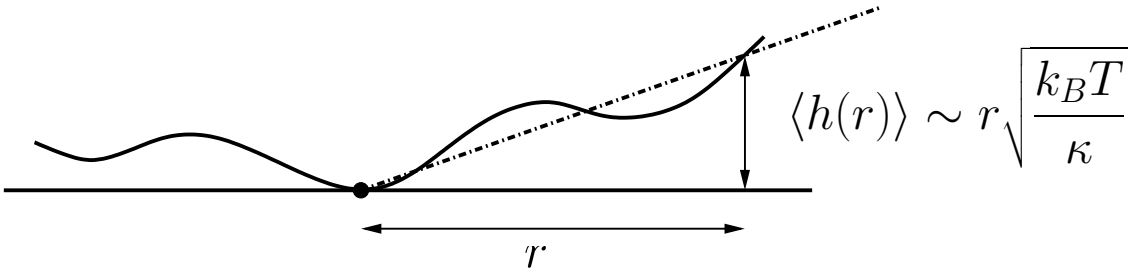

Figure 1.5: The fact that the statistics of thermal height fluctuations is not affected by the single pinning point implies that the typical height of the fluctuations scales linearly with the distance from the pinning site. (Adapted from [40])

does not modify the membrane spectrum of thermal fluctuations (eq. 1.5). The pinning point and the surface only eliminate the membrane translational degree of freedom (by enforcing the global minimum of the membrane height function to be located at the point of contact with the surface) and, therefore, the attachment free-energy cost is given by the above eq. 1.7. The fact that the fluctuations spectrum is identical to that of a free membrane implies that, the typical mean height at which the membrane undulates above the surface at a distance r away from the pinning point scales linearly with r [41, 43]:

$$u(r) \equiv \langle h(r) \rangle \sim r\sqrt{\frac{k_B T}{\kappa}}, \tag{1.8}$$

which illustrate in fig. 1.5. There is repulsive force acting between the fluctuating membrane and the underlying surface, caused by their mutual steric hindrance. Helfrich [44] showed that the associated repulsive interaction free energy density (per unit area) has the following scaling behavior $V(r) \sim (k_B T)^2/\kappa u(r)^2$ which, together with eq. 1.8, yields

$$V(r) \sim \frac{k_B T}{r^2}. \tag{1.9}$$

By integrating this energy density over the projected area of the membrane, one derives

eq. 1.7 up to a numerical prefactor

$$F_1 = \int V(r) d^2\vec{r} \sim \int_l^L 2\pi r \frac{k_B T}{r^2} dr = C k_B T \ln\left(\frac{L}{l}\right). \tag{1.10}$$

To set $C = 2$, as in eq. 1.7, one needs to replace the scaling relation eq. 1.9 with the equality

$$V(r) = \frac{k_B T}{\pi r^2}. \tag{1.11}$$

The free energy density of eq. 1.11 due to the steric hindrance between the fluctuating membrane and the surface, is directly related to the rate of collisions between them. In other words, the probability density that the membrane hits the supporting surface at a distance r from the pinning point exhibit the same dependence on r vs $V(r)$:

$$p\left[h(\vec{r}) = 0\right] \sim \frac{1}{r^2}. \tag{1.12}$$

The relationship between the thermal fluctuations and the collisions rate provides the information needed for calculating the fluctuation induced attractive potential between two adhesion bonds. This is done by regarding the point of collision between the membrane and the surface as a second pinning point which can diffuse across the surface. In this context, the probability density $p\left[h(\vec{r}) = 0\right]$ is identified with the pair correlation function between the adhesion bonds which, therefore, also follows the scaling form

$$g(\vec{r}) \sim \frac{1}{r^2}. \tag{1.13}$$

By definition, the pair potential of mean force is given by

$$U(\vec{r}) \equiv -k_B T \ln\left[g(\vec{r})\right] = 2 k_B T \ln\left(r\right), \tag{1.14}$$

which is an infinitely long range attractive potential that does not depend of the bending

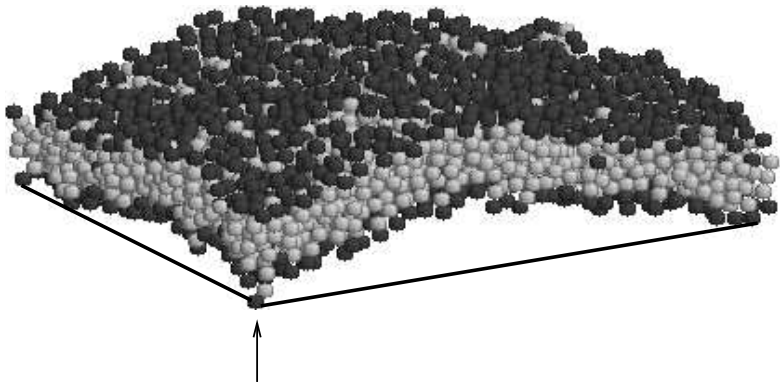

Figure 1.6: Equilibrium configuration of a membrane consisting of 2000 lipids. Each lipid is represented by a trimer of one hydrophilic bead (dark gray sphere) and two "hydrophobic" beads (light gray spheres). The membrane is fluctuating above a plane surface (frame indicated by a thick black line), while one of the hydrophilic beads (the black sphere appearing at the front of the figure and indicated by an arrow) is held on the surface at a fixed position. (Adapted from [18])

rigidity of the membrane, κ.

The validity of eq. 1.13 had been tested by Farago [42], using MC simulations of the ISCG (implicit-solvent coarse-grained) model shown in fig. 1.6 with two lipid heads attached to surface - one fixed at the origin and the other allowed to diffuse on the flat surface. The pair correlation function is then directly computed by sampling the position of the mobile adhesion bond. The results [42], which are shown in fig. 1.7, agree very well with eq. 1.13. The slope of the straight line on the log-log plot is equal to -2. The deviations from the power law behavior $g(\vec{r}) \sim 1/r^2$ at small values of r ($r/L < 0.05$) are related to the breakdown of the continuum description of the Helfrich Hamiltonian at small spatial scales. At small separations, the molecular nature of the lipids becomes important and the radial pair distribution function is dominated by the depletion shells around the lipids.

1.3.3 Membrane with multiple adhesion bonds

The fundamental difficulty in attempting to provide a statistical-mechanical analysis of the aggregation behavior of the adhesion bonds is the need to integrate out the membrane degrees of freedom and write down the potential of mean force as a function of the coordinates of

the adhesion sites $U(\vec{r}_1, \vec{r}_2, \vec{r}_3, \ldots, \vec{r}_N)$. This is a non-trivial problem since the membrane-

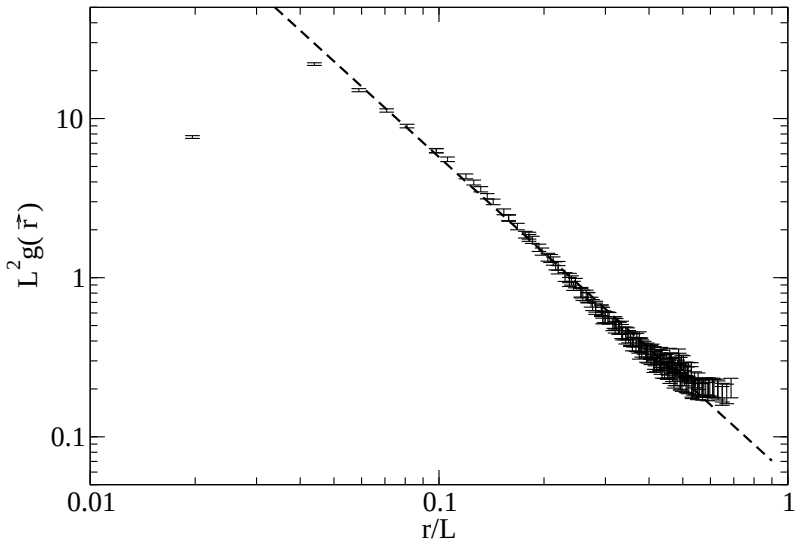

Figure 1.7: The pair correlation function, $g(\vec{r})$, of a non-stressed membrane vs. the pair distance r. The slope of the dashed straight line is -2. (Adapted from [42])

mediated potential $U(\vec{r}_1, \vec{r}_2, \vec{r}_3, \ldots, \vec{r}_N)$ is a many-body potential which cannot be expressed as the sum of two body terms(as oppose to electrostatic potential) of the form in eq. 1.14. The many-body nature of $U(\vec{r}_1, \vec{r}_2, \vec{r}_3, \ldots, \vec{r}_N)$ is best illustrated by the following example: Consider the configuration shown in fig. 1.8(A) with two adhesion bonds at located at $\vec{r_1}$ and $\vec{r_2}$ and, in comparison, the one shown in fig. 1.8(B) with a single bond at $\vec{r_1}$ and a cluster of three bonds around $\vec{r_2}$. Clearly, the spectrum of membrane thermal fluctuations in both cases is quite the same and, therefore, the adhesion bond located at $\vec{r_1}$ is attracted to the three-point cluster in 1.8(B) by the same force to which it is attracted to the single adhesion bond in 1.8(A). If $U(\vec{r}_1, \vec{r}_2, \vec{r}_3, \ldots, \vec{r}_N)$ was the sum of pair interactions, the force in fig. 1.8(B) would be three times larger than the force in 1.8(A). We will present our solution to this problem in chapter 2.

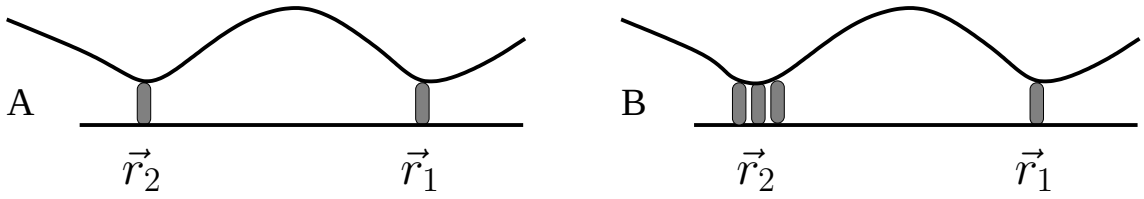

Figure 1.8: (A) Schematic of a supported membrane with two adhesion located at $\vec{r_1}$ and $\vec{r_2}$. (B) Similar to (A), but with a three-bond cluster instead of a single adhesion bond in $\vec{r_2}$. The adhesion bond in $\vec{r_1}$ is equally attracted (by a Casimir-like force) to the adhesion bond located in $\vec{r_2}$ in (A) and to the cluster of three adhesion bonds shown in (B). (Adapted from [40])

1.4 Outline

The thesis is organized as follows: In chapter 2 we present an accurate approach to the problem of the fluctuation-induced many-body potential, which employs a non-additive many-body potential $U(\vec{r}_1, \vec{r}_2, \vec{r}_3, \ldots, \vec{r}_N)$. We will integrate out the membrane degrees of freedom and map the problem onto a lattice gas model where the occupied sites represent the adhesion bonds. We will present a mean-field analysis and MC simulations of our model and show that, while the fluctuation-mediated interactions alone are not sufficient to allow the formation of aggregation clusters, they greatly reduce the strength of the residual (direct) interactions between adhesion bonds which is required to facilitate cluster formation. Further on, in chapter 3, we will study the formation of adhesion domains in cellular membranes which also include trans-membrane proteins. We will calculate the inclusion-adhesion bond pair distribution function and show that in contrast to the weak attraction between two adhesion bonds (see ref. [42]), the fluctuation-induced attraction between the adhesion bond and a large inclusion is sufficiently strong to keep the adhesion bond in the vicinity of the inclusion. We will also study the distribution and aggregation of many adhesion bonds around the inclusion and show that, the attraction of adhesion bonds towards the inclusion is strongly self-screened. In chapter 4 we summarize the results and discuss future open questions.

Chapter 2

Condensation of adhesion domains of supported membranes

The exact form of the fluctuation-mediated many-body potential $U(\vec{r}_1, \vec{r}_2, \vec{r}_3, \ldots, \vec{r}_N)$ is still an open question that needs to be resolved for the fluctuation-induced domain formation to be understood. Several approximations to this problem which avoid direct many-body calculations have been proposed. Weikl and Lipowsky introduced a theory in which the effect of the pinning points is represented by a *homogeneous* attractive interaction between the fluctuating membrane and the underlying surface (or between the membrane and another membrane) [45]. They concluded that the homogeneous fluctuation-induced potential alone cannot facilitate the formation of adhesion zones, but it greatly reduces the critical strength of the residual interactions between the adhesion bonds above which the formation of adhesion clusters is possible. A very similar conclusion has been recently reached by Speck, using rigorous statistical mechanical methods [46]. However, in his model the hard-wall interaction between the membrane and the surface has been replaced with a harmonic confining potential.In this thesis, we present a more accurate approach to the problem which employs a non-additive many-body potential $U(\vec{r}_1, \vec{r}_2, \vec{r}_3, \ldots, \vec{r}_N)$.

2.1 The many-body fluctuation-mediated potential

2.1.1 The many-body problem

In order to find the exact form of the many-body fluctuation-mediated potential, we start our argument by focusing on the results presented in fig. 1.7. These results were derived from MC simulations with periodic boundary conditions, which mean that each of the two adhesion bonds (mobile and fixed) has three periodic images. (In fact, each adhesion bond has infinite array of periodic images.) Accordingly, in the simulations, the variable r (see x-axis in fig. 1.7) represents the distance to the nearest periodic image, as routinely done in computer simulations. The fact that the pair potential of mean force between two adhesion bonds is an infinitely long range attractive potential (see eq. 1.14), raises the following puzzle: If the potential is felt at large distances, all the periodic images are expected to influence the pair correlation function between the adhesion bonds. Nevertheless, there is a pretty good agreement between the MC results and eq. 1.13, which has been derive for only two adhesion bonds. The only possible way to explain this surprising observation is to assume that the periodic images of the adhesion bonds are largely screened and only the nearest image is felt. This assumption is consistent with the following physical picture: The membrane mediated interactions originate from the entropic cost due to the suppression of the membrane thermal undulations. Thus, the presence of each adhesion bond is felt only in the region where it affects the fluctuations and cause their reduction, while outside of this region, the adhesion bond is effectively screened.

In this perspective, the idea that distant adhesion bonds are screened seems logical. The fluctuations vanish at each adhesion bond, irrespective of the distribution of the others. Moreover, in the immediate vicinity of each adhesion bond, one expects the amplitude of the fluctuations to depend only on the distance from that adhesion bond. For tensionless membrane, the amplitude of the fluctuations in this region grows linearly with the distance r from the adhesion bond, as given by eq. 1.8. We now wish to introduce a more general

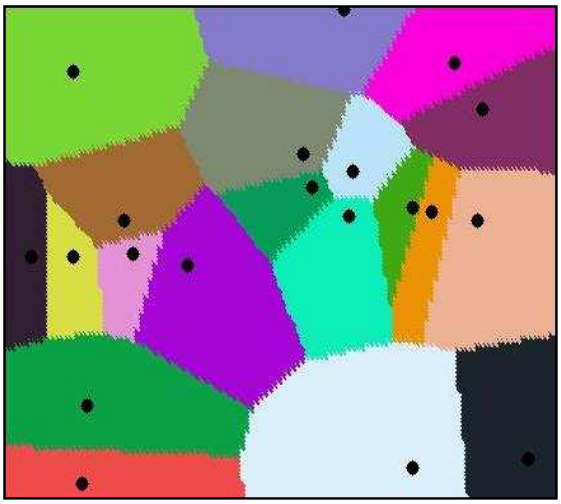

Figure 2.1: Example of the Voronoi diagram where the black dotes represent the adhesion bonds. Each color represent a membrane area that its local fluctuation is governed by its inner adhesion bond (Voronoi cell).

expression that holds over the entire area of the membrane and coincides with eq. 1.8 close to every adhesion bond. Our suggestion is as follows [47]: In each unit area of the membrane, the mean height of the membrane above the surface is given by

$$\langle h(r) \rangle \sim d_{min} \sqrt{\frac{k_B T}{\kappa}}, \tag{2.1}$$

where d_{min} is the distance of the unit area from the nearest adhesion bond. We also replace r with d_{min} in eq. 1.11 for the attachment free energy density, which now reads

$$V(r) = \frac{1}{\pi} \frac{k_B T}{d_{min}^2} \tag{2.2}$$

The total attachment free energy of a given distribution of adhesion bonds is obtained by integrating the attachment free energy density eq. 2.2 over the entire membrane area. This calculation is done by constructing the 2D Voronoi diagram of the distribution of N adhesion bonds (see fig. 2.1), integrating the free energy density with each cell (where in each cell the distance is measured from the adhesion bond located in the cell, and a small region of microscopic size l around the bond is excluded from the integral), and summing

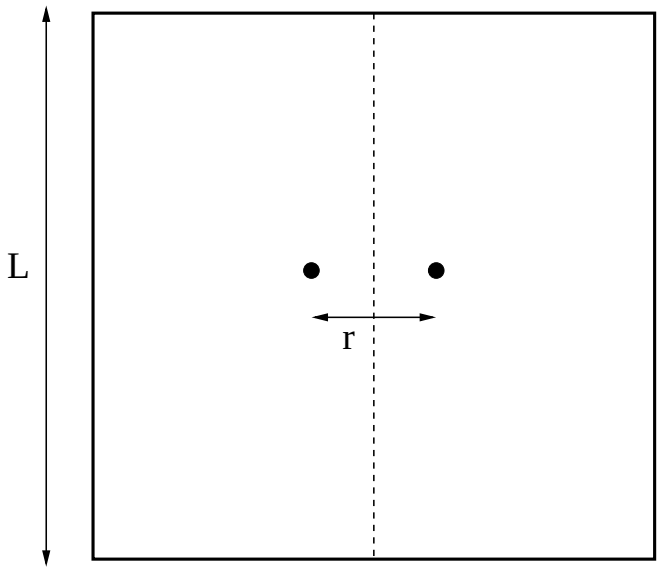

Figure 2.2: Schematic of a square membrane of linear size L with two adhesion bonds located at $(x, y) = (\pm r/2, 0)$. the dashed line shows thw boarder between the governed areas of the adhesion bonds. (Adapted from [40])

the contributions of the different cells:

$$F_N = \sum_{i=1}^{N_{cell}} \int \frac{k_B T}{\pi r^2} d^2\vec{r}. \tag{2.3}$$

2.1.2 The two-body problem revisited

Let us see how one can re-derive eq. 1.14 for the pair potential of mean force by calculating the attachment free energy eq. 2.3. We consider the membrane shown schematically in fig. 2.2 with two adhesion bonds, where each of which located a distance $r/2$ from the center of the membrane. The dashed line shows the boarder between the Voronoi cells of the adhesion bonds, where each cell extends over half of the area of the membrane. For the configuration shown in fig. 2.2, the attachment free energy eq. 2.3 reads:

$$F_2 = 4\int_0^{L/2} dy \left[\int_0^{(r-l)/2} dx \, \frac{k_B T}{\pi \left[y^2 + (x - r/2)^2 \right]} + \int_{(r+l)/2}^{L/2} dx \, \frac{k_B T}{\pi \left[y^2 + (x - r/2)^2 \right]} \right]. \tag{2.4}$$

Integrating over y yields,

$$F_2 = \frac{4k_B T}{\pi} \left[\int_0^{(r-l)/2} \frac{dx}{|x - r/2|} \tan^{-1}\left(\frac{L}{2|x - r/2|} \right) + \int_{(r+l)/2}^{L/2} \frac{dx}{|x - r/2|} \tan^{-1}\left(\frac{L}{2|x - r/2|} \right) \right]. \tag{2.5}$$

Assuming that $l < r \ll L$, the inverse tangent function in eq. 2.5 can be approximated by the constant value of $\pi/2$ over most of the integration range. With this approximation, one gets

$$F_2(r, L) \simeq 2k_B T \ln\left(\frac{L}{l} \right) + 2k_B T \ln\left(\frac{r}{l} \right) = F_1(L) + U(r). \tag{2.6}$$

The first term in eq. 2.6 is the free energy cost of a single adhesion site [eq. 1.7], which is the expected value when the two adhesion bonds coincide ($r \simeq l$) to form a single cluster. The second term, which represents the additional free energy cost associated with the separation of the adhesion bonds, is identified as the fluctuation induced pair potential, in agreement with eq. 1.14. Eq. 2.6 demonstrated that the attachment free energy and the potential of mean-force are equal to each other, up to a constant which is the attachment free energy of a single bond:

$$U(\vec{r}_1, \vec{r}_2, \vec{r}_3, \ldots, \vec{r}_N) = F_N(\vec{r}_1, \vec{r}_2, \vec{r}_3, \ldots, \vec{r}_N, L) - F_1(L). \tag{2.7}$$

2.2 Lattice-gas model for adhesion bonds in supported membrane

How different is the formation of adhesion domain in supported membrane from a conventional gas to liquid condensation in 2D systems? The liquid-gas phase transition can be analyzed in the framework of an Ising-like model of identical particles that populate a lattice (see fig 2.3). Excluded volume interactions between particles are represented by the fact each lattice site can be occupied by no more than one adhesion point. When two particles occupy nearest-neighbor sites, they interact in a pairwise fashion with an attractive energy $-\epsilon$. Denoting the occupancy of a lattice site by s_i, with $s_i = 0$ for an empty site and $s_i = 1$ for an occupied site, the Hamiltonian of the lattice-gas model is given by

$$\mathcal{H}_{\rm LG} = \sum_{\langle i,j \rangle} -\epsilon s_i s_j, \tag{2.8}$$

where the sum runs over all the pairs of lattice nearest neighbor sites. The phase diagram of the lattice-gas model is well known. There exists a critical value α_c such that if the interaction energy $\epsilon < \alpha_c k_B T$, the particles will be distributed uniformly within the lattice. Above this critical value, $\epsilon > \alpha_c k_B T$, a uniform distribution of the particles is observed only at low concentrations of particles ("gas phase"), but upon increasing the concentration of particles, the system undergoes a first order phase transition and a second coexisting phase appears with a considerably larger concentration ("condensed phase").

In supported membranes with adhesion bonds, the short range interactions introduces in $\mathcal{H}_{\rm LG}$ (eq. 2.8) may originated from depletion and hydrophobic interactions between the adhesion bonds [37]. In addition, the adhesion bonds interact via the fluctuation-induced potential of mean-force, given in eqs. 2.3. The discrete analog of eq. 2.3, is given by

$$F_N = \sum_{i=1}^{N} \frac{k_B T}{\pi} \left(\frac{l}{d_{min}} \right)^2 (1 - s_i), \tag{2.9}$$

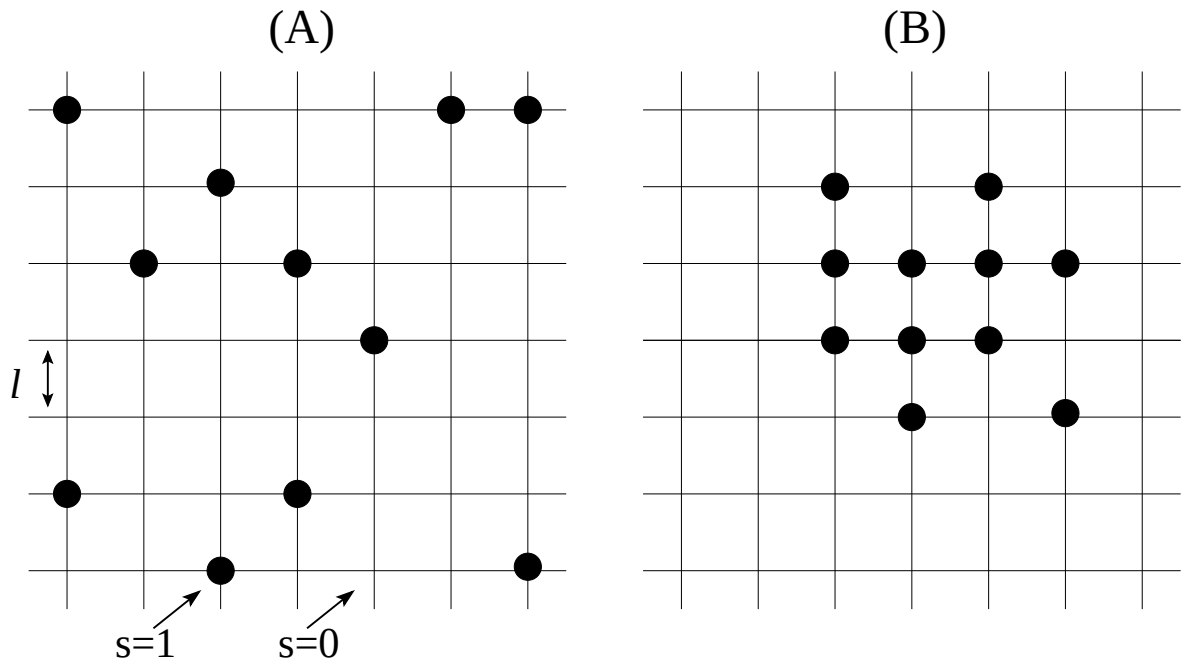

Figure 2.3: Example of the lattice-gas model with lattice spacing equal to l. The occupied and the empty sites denoted by $s = 1$ and $s = 0$, respectively. (A) represent a gas phase while (B) represent a liquid-like phase.

where d_{min} is the distance from a vacant lattice site to the nearest occupied lattice site and l^2 is the area per lattice site. Notice that only the vacant lattice sites, that represent the unit areas of the fluctuating membrane, contribute to the sum. Introducing eq. 2.9 into eq. 2.8, we arrive to the Hamiltonian for our lattice model of adhesion bonds,

$$\mathcal{H} = \sum_{\langle i,j \rangle} -\epsilon s_i s_j + \sum_{i=1}^{N} \frac{k_B T}{\pi} \left(\frac{l}{d_{min}} \right)^2 (1 - s_i). \tag{2.10}$$

2.3 Mean-field theory

In this section, we present a mean field analysis of our model depicted by eq. 2.10. Let us consider a lattice of N_s sites of which $N \leq N_s$ sites are occupied by adhesion points. Let us further assume that the adhesion points form $N_c \leq N$ adhesion clusters. The free energy of system includes three contributions: (i) the mixing entropy of the adhesion clusters, $F_{\rm mix}$, (ii) the lattice-gas energy, $E_{\rm LG}$, of the direct interactions between the adhesion points [first

term in eq. 2.10], and (iii) the attachment free energy, F_N [second term in eq. 2.10]. The first free energy contribution is given by

$$\frac{F_{\rm mix}}{k_BT} = N_c\left[\ln\left(\frac{N_c}{N_s}\right) - 1\right] + \frac{1}{2}c\left(\frac{N_c^2}{N_s}\right), \tag{2.11}$$

where c is the second virial coefficient. On average, each cluster consists of (N/N_c) adhesion points; and if we assume that it has a roughly circular shape than $c \simeq 4(N/N_c)$. Denoting the number densities of the adhesion points by $\phi = N/N_s$, and of the clusters by $\phi^* = N_c/N_s \leq \phi$, the free energy of mixing per lattice site is given by

$$\frac{F_{\rm mix}}{N_s k_BT} = \phi^*\left[\ln\left(\phi^*\right) - 1\right] + 2\phi\phi^*. \tag{2.12}$$

The second contribution to the free energy is due to the direct interactions between the adhesion points. The ground state of the interaction energy $E_{\rm LG}$ is achieved when a single circular adhesion domain with minimal surface is formed. If we set the ground state as the reference energy, the energy of an ensemble of clusters can be estimated as being proportional to the total length of the domain boundaries. For N_c circular clusters of size (N/N_c) we have

$$\frac{E_{\rm LG}}{N_s k_BT} = \lambda\frac{N_c}{N_s}\sqrt{\frac{N}{N_c}} = \lambda\sqrt{\phi\phi^*}, \tag{2.13}$$

where λ, the associated dimensionless line tension, is proportional to the interaction energy ϵ in eq. 2.10 and B, the mean number of nearest-neighbor vacant sites per occupied site on the boundary of a cluster ($B \to 1$ for very large clusters),

$$\lambda = 2\sqrt{\pi}B\epsilon. \tag{2.14}$$

The sum of free-energy contributions (2.12) and (2.13) constitutes the total free-energy

density (per lattice site) of a 2D lattice gas of clusters

$$\frac{F_{\mathrm{LG}}}{N_s k_B T} = \phi^* \ln(\phi^*) - \phi^* + 2\phi\phi^* + \lambda\sqrt{\phi\phi^*}. \tag{2.15}$$

The third contribution of the attachment free energy can be estimated as follows. The clusters form N_c Voronoi cells, each of which has on average an area of $A_{\mathrm{vor}} = (N_s/N_c)l^2$. The attachment free energy of each Voroni cell is given an equation similar to eq. 1.7 for the attachment free energy of one adhesion point, but with A_{vor} instead of the total membrane area L^2. Thus

$$F_N = N_c \left[k_B T \ln\left(\frac{N_s}{N_c}\right)\right], \tag{2.16}$$

and the attachment free energy density is given by

$$\frac{F_N}{N_s k_B T} = -\phi^* \ln(\phi^*), \tag{2.17}$$

which eliminates the first term in the lattice-gas free energy density (eq. 2.15), yielding

$$\frac{F}{N_s k_B T} = \frac{F_{\mathrm{LG}}}{N_s k_B T} + \frac{F_N}{N_s k_B T} = -\phi^* + 2\phi\phi^* + \lambda\sqrt{\phi\phi^*}. \tag{2.18}$$

We consider a low density of adhesion sites $\phi \ll 1$, which also implies a low number density of adhesion clusters since $\phi^* \leq \phi$. By minimizing the free energy density we obtain the equilibrium value of the ϕ^* for the lattice-gas problem (eq. 2.15) and for the adhesion points of a fluctuating supported membrane (eq. 2.18). In both cases, the system undergoes a first order phase transition at $\lambda_1(\phi)$ from the gas phase ($\phi^* = \phi$) to a condensed phase consisting of only a few clusters ($\phi^* \sim 0$). Also, in both cases the free energy reaches a maximum at intermediate densities ($0 < \phi^* < \phi$). This free energy barrier for condensation

disappears at the spinodal point $\lambda_2(\phi) > \lambda_1(\phi)$. For the lattice-gas problem we find

$$\begin{aligned} \lambda_1^{\mathrm{LG}} &= 1 - 2\phi - \ln(\phi) \\ \lambda_2^{\mathrm{LG}} &= -4\phi - 2\ln(\phi), \end{aligned} \tag{2.19}$$

while for the adhesion points of fluctuating membranes we have

$$\begin{aligned} \lambda_1 &= 1 - 2\phi \\ \lambda_2 &= 2 - 4\phi = 2\lambda_1. \end{aligned} \tag{2.20}$$

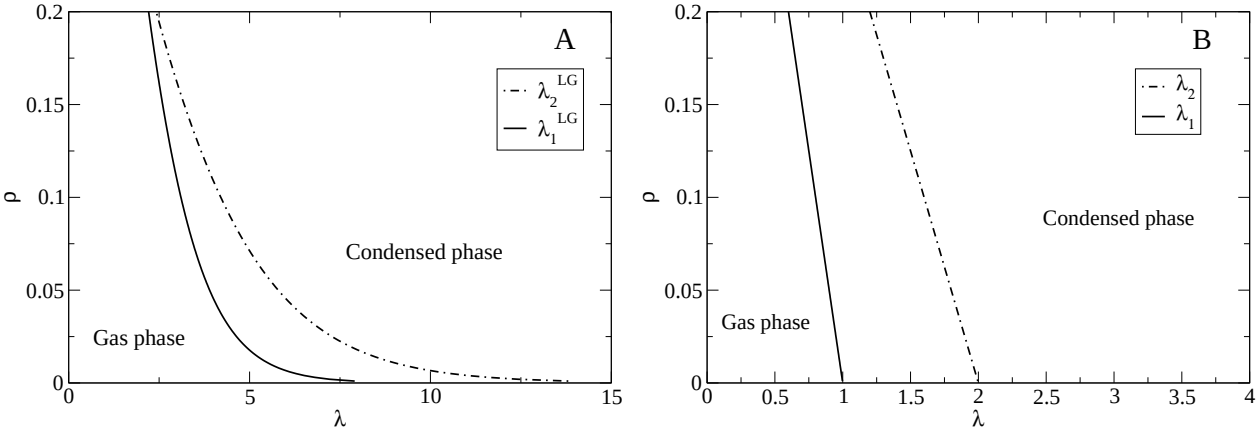

Figure 2.4: The phase diagram of the adhesion sites calculated within the mean field approximation eqs. 2.19 and 2.20. λ_1 and λ_2 represent the first-order transition and spinodal lines, respectively. (Adapted from [47])

The results of eqs.(2.19) and (2.20) are summarized in fig. 2.4A and B, respectively. The important points in the results are that: i) $\lambda_1 > 0$, which means that the fluctuation induced interactions alone are not sufficient to induce aggregation of adhesion domains, but ii) they greatly reduce the strength of the direct interactions required to facilitate cluster formation since $\lambda_1 < \lambda_1^{\mathrm{LG}}$ (and also $\lambda_2 < \lambda_2^{\mathrm{LG}}$). In the following section we support these conclusions with MC simulations. We show that for adhesion points of fluctuating membranes, the site-site cohesive energy ϵ for the onset of aggregation falls below the thermal energy $k_B T$.

2.4 Computer simulations

To further investigate the aggregation behavior of adhesion points, we performed MC simulations of our lattice gas model with the total configurational energy given by the sum of direct (eq. 2.8) and fluctuation-induced (eq. 2.9) interactions. We used a 120×138 triangular lattice (that has an aspect ratio very close to 1) with periodic boundary conditions. We simulated the system at two different densities $\phi = N/N_s = 0.05$ and $\phi = 0.1$, and for various values of ϵ ranging from 0 to 3 k_BT. For comparison, we also simulated the standard lattice gas model (for which the configurational energy is given by eq. 2.8, without the fluctuation-mediated free energy eq. 2.9). For each density ϕ and for each value of ϵ, we performed 8-16 independent runs starting from different initial configurations where the points are either randomly distributed on the lattice (as in fig. 2.5A) or put in a single cluster (see fig. 2.5B). The system was then equilibrated until the distribution of points in all the independent runs looks similar (see e.g., fig. 2.5C vs. D, and fig. 2.5E vs. F). Equilibrium time for the different samples ranges from 3.6×10^5 to 10^6 MC time units, where each MC time unit consists of N single particle move attempts. For the adhesion points problem, each particle was displaced to a randomly chosen nearest neighbor lattice site, which enabled us to employ an efficient algorithm to update the Voronoi diagram needed for calculating the fluctuation-mediated free energy (2.9). For the standard lattice gas model, each move attempt consisted of randomly selecting a particle and moving it to the nearest vacant point in a randomly chosen lattice direction[1]. After the first stage of equilibration, the simulations were continued for 3×10^5 MC time units during which data was collected every third MC time unit.

To examine the occurrence of a phase transition from a gas to a condensed phase, we measured the average number of clusters in the system (where a cluster is defined as a set of neighboring occupied sites), and the mean value of the energy of direct interactions between

[1]Such MC moves greatly reduce the rejection probability due to excluded volume interaction. One can easily verify that for these moves, detailed balanced is satisfied by the conventional Metropolis acceptance rule $p(\text{old} \to \text{new}) = \min(1, \exp(-\Delta E/k_BT))$, where ΔE is the energy change caused by the move attempt.

sites, $\langle E_{\rm LG} \rangle$ (see eq. 2.8). Our results are summarized in fig. 2.6A (for $\phi = 0.05$) and B (for $\phi = 0.1$). For each ϕ we measured these quantities both for the standard lattice gas model (open symbols and dash-dotted lines in fig. 2.6) and for adhesion points which also interact via the fluctuation-mediated free energy eq. 2.9 (solid symbols and solid lines in fig. 2.6). The number of clusters is denoted by squares (values on the right y-axis of the figures), while $\langle E_{\rm LG} \rangle$ is represented by circles (values on the left y-axis).

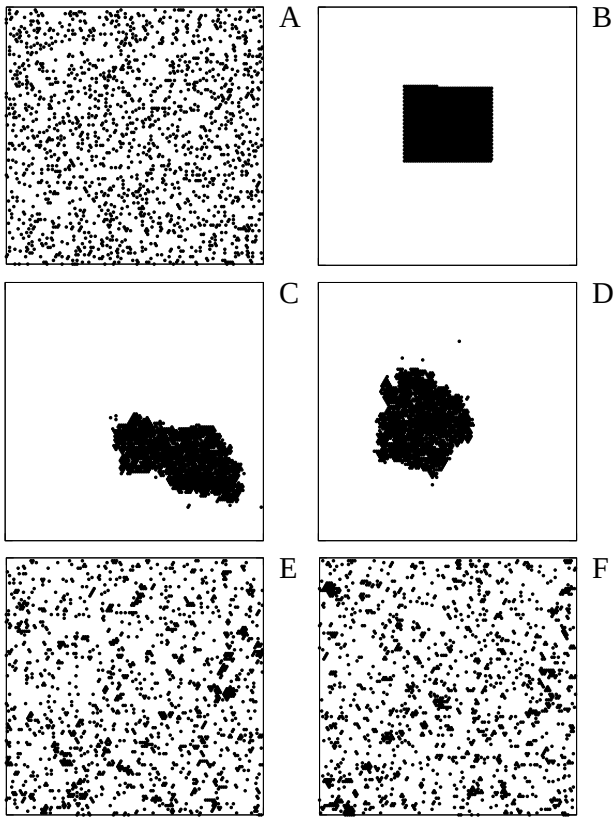

Figure 2.5: Initial configurations of the simulations in which (A) the sites are randomly distributed on the lattice, and (B) put in a single compact cluster. Representative equilibrium configurations of (C-D) our model (eqs. 2.8 and 2.9 and (E-F) the standard lattice-gas model (eq. 2.8 only) for $\phi = 0.1$ and $\epsilon = 1 k_B T$. Configurations (C) and (E) evolved from the initial state (A), while (D) and (F) evolved from (B). (Adapted from [47])

The gas phase is characterized by a large number of small clusters, some of which may be of the size of a single site. Furthermore, since each occupied site has a relatively small number of neighboring occupied sites, the mean configurational energy $\langle -E_{\rm LG} \rangle$ is relatively low. Conversely, when the sites form large clusters in the condensed phase, $\langle -E_{\rm LG} \rangle$ is high,

and the total number of clusters decreases (and in many cases, especially for large values of ϵ, we simply observe only a single cluster in our system). Figure 2.6 exhibits an abrupt, clearly first-order, transition from a gas phase with a large number of clusters and small $\langle -E_{\rm LG} \rangle$ to a condensed state with a small number of clusters and large $\langle -E_{\rm LG} \rangle$. The estimated

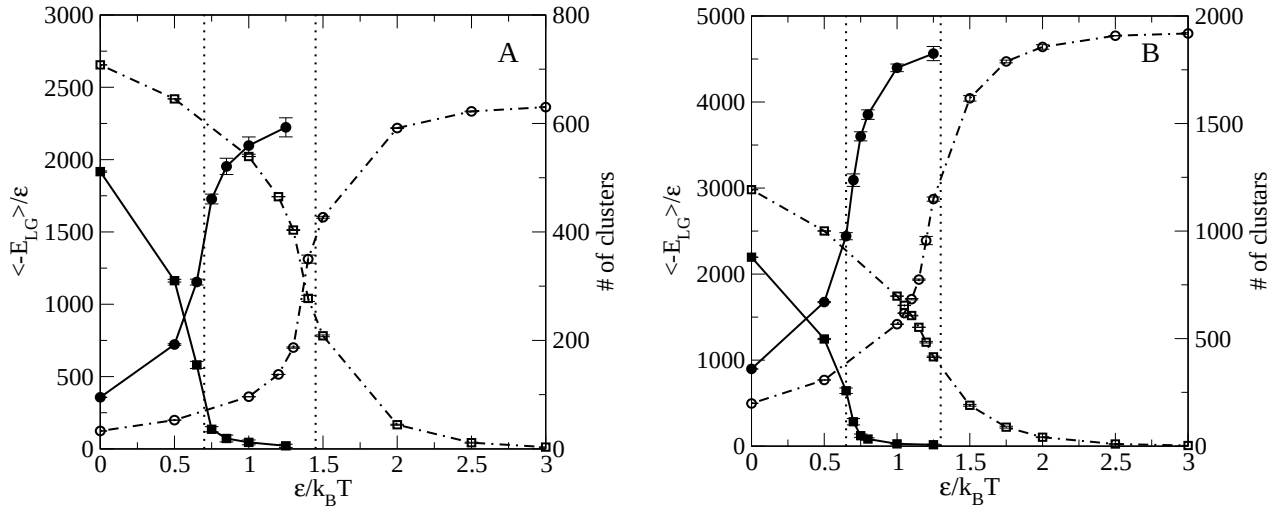

Figure 2.6: Left y-axis: The energy of direct interactions between sites, $\langle E_{\rm LG} \rangle$ (eq. 2.8) as a function of ϵ, for $\phi = 0.05$ (A) and $\phi = 0.1$ (B). Solid circles - results for our model for adhesion points. Open circles - results for the standard lattice-gas model. Right y-axis: The number of clusters as a function of ϵ, for $\phi = 0.05$ (A) and $\phi = 0.1$ (B). Solid squares - results for our model for adhesion points. Open squares - results for the standard lattice-gas model. (Adapted from [47])

values of ϵ at the transition are (see vertical lines in fig. 2.6): $\epsilon_t \simeq 0.7 k_B T$ ($\phi = 0.05$) and $\epsilon_t \simeq 0.65 k_B T$ ($\phi = 0.1$). In comparison (see also fig. 2.6), for the standard lattice gas model, the transition values are roughly twice larger than these values: $\epsilon_t^{\rm LG} \simeq 1.45 k_B T$ ($\phi = 0.05$) and $\epsilon_t^{\rm LG} \sim 1.3 k_B T$ ($\phi = 0.1$). Figure 2.5C-F exhibit typical equilibrium configurations of the system at $\phi = 0.1$ and $\epsilon = 1 k_B T$. For the lattice gas model $\epsilon_t^{\rm LG} > 1 k_B T$, and at equilibrium the system is in the gas phase (figs. 2.5E and F). When the fluctuation-induced interactions eq. 2.9 are introduced, ϵ_t falls below $1 k_B T$ and the system is in the condensed phase where most of the particles belong to one large cluster (figs. 2.5C and D).

Our computational results, which show that the fluctuation-mediated interactions re-

duce the strength of ϵ_t, are in a qualitative agreement with the mean-field theory prediction (sect. 2.3). To make a quantitative comparison between the theory and the simulations, one needs to estimate the parameter B appearing in eq. 2.14. Several reasons make such an estimation difficult and inaccurate: First, our non-standard mean-field theory is based on the assumption that the clusters are circular and roughly have the same size, which is quite a crude approximation. Second, tracing the precise location of ϵ_t in fig. 2.6 is largely inaccurate because of the finite size of the system that makes the transition look like a crossover. To reduce the large uncertainties associated with the determination of ϵ_t, one can look at the difference between the value of this quantity in our model and for the standard lattice gas model. Using

$$\lambda_1^{\mathrm{LG}} - \lambda_1 = 2\sqrt{\pi} B \left(\epsilon_t^{\mathrm{LG}} - \epsilon_t\right), \tag{2.21}$$

for $\phi = 0.1$, we find $B \simeq 1$, as indeed expected for large clusters.

2.5 Summary

In this chapter we studied the aggregation behavior of adhesion points between a fluctuating membrane and a supporting surface. We demonstrated that the problem can be mapped onto a lattice gas model with two types of molecular interactions: i) direct site-site pair interactions and ii) Casimir-like interactions which are mediated by the membrane thermal fluctuations. The fluctuation-mediated interactions, which are inherently of many-body character, are calculated in our model by summing over the vacant rather than the occupied sites of the lattice. Each vacant site represents a small unit area of the fluctuating membrane, and the fluctuation-mediated potential expresses the local free-energy cost due to the restriction imposed by the adhesion points on the membrane thermal fluctuations. This free-energy cost depends mainly on the distance between the vacant sites and the nearest occupied site. Therefore, such a many-body potential is calculated by determining the Voronoi diagram for

each lattice configuration, which can be quite easily implemented in MC simulations.

We used mean-field calculations and MC computer simulations to investigate the phase behavior of a lattice gas of adhesion sites at low densities. We showed that upon increasing the strength of the site-site interactions ϵ, the system undergoes a first-order phase transition into a condensed state. The fluctuation-induced interactions lower the value of ϵ at the phase transition to below the thermal energy k_BT. This result suggests that fluctuation-mediated effects play a central role in the formation of adhesion domains in biomimetic and biological membranes.

Chapter 3

Entropic attraction of adhesion bonds towards cell boundaries

In the previous chapter we looked on the aggregation behavior of adhesion bonds in biomimetic supported membranes. Cellular membranes consist of various structure complexes and include a variety of trans-membrane proteins necessary for different biological functions. In this chapter we investigate how the presence of membrane proteins (inclusions) effects the formation of adhesion domains[1]. Membrane inclusions tend to reduce the amplitude of the thermal fluctuations and, therefore, they are likely to modify the fluctuation-induced aggregation behavior of adhesion bonds. In this context, it is worthwhile to mention that there is a great bulk of experimental [10, 48, 49] and theoretical [50–53] works on the fluctuation-mediated potential between the inclusions themselves. Here, we tackle a different problem and explore how a single inclusion affects the aggregation of adhesion bonds. Since the formation of adhesion cluster is driven by the tendency to localize the reduction of the thermal fluctuations in a restricted area, it is natural to expect that adhesion bonds would exhibit

[1]Two important remarks: (i) The distinction between "proteins" and "adhesion bonds" is somewhat academic since the receptor and ligand molecules may themselves be proteins. Thus, we are essentially interested in domains consisting of proteins of different sizes and functions. (ii) The formation of adhesion complexes, like focal adhesion, is also largely influenced by active processes involving the cytoskeleton. Here, we are interested in the direct and membrane-mediated interactions within the complex, and it remains to be seen how the cytoskeleton can be integrated into our models.

affinity to the surface of the inclusion. Physically, the effect of an inclusion on the thermal fluctuations should be similar to that of a cluster of adhesion bonds of the same size. However, as discussed above, without direct residual interactions the system is in the gas-phase and a cluster of adhesion bonds is not stable. Therefore, the presence of the inclusion is not equivalent to the formation of a cluster, which is only transient.

3.1 The bond-inclusion pair interaction

We consider the model system shown schematically in fig. 3.1, consisting of a circular membrane of radius L, a circular inclusion of radius $r_0 \ll L$ fixed at the center of the membrane, and a single adhesion bond located at $\vec{r}$. The total attachment free energy of the system is given by (see eq. 2.3)

$$F(\vec{r}, r_0, L) = \int_{r_0+l}^{L-l} \frac{k_B T}{\pi d_{\min}^2(\vec{r'}, \vec{r}, r_0, L)} d\vec{r'}, \tag{3.1}$$

where the integration is carried over the whole area of the membrane, excluding regions of microscopic size l near the inner ($|\vec{r'}| = r_0$) and outer ($|\vec{r'}| = L$) boundaries, and in the vicinity of the adhesion bond ($\vec{r'} = \vec{r}$). In eq. 3.1, $d_{\min}$ denotes the distance of a given point $\vec{r'}$ on the membrane to the nearest "obstacle", which may be either the adhesion bond or the surface of the inclusion. The assumption underlying eq. 3.1 is that the membrane separation at the inclusion is the same as the length of the adhesion bond. Had there been a length mismatch between the inclusion and the adhesion bonds, it would have bending elasticity energy cost that weakens the fluctuation-induced attraction. In a binary mixture of adhesion bonds, the inclusion is likely to have a higher affinity to the adhesion bonds with the smaller length mismatch, which may lead to phase segregation in the mixture [55, 56].

In what follows, we consider membranes with both "open" and "closed" outer boundaries. At a closed boundary, the membrane is attached to a frame, whereas at an open boundary, the membrane fluctuates freely. Thus, the former is also considered as an obsta-

cle, while the latter is not. The open and closed boundary conditions represent two limiting cases. Cellular membranes are attached to the actin cytoskeleton located mainly at the periphery of the cell., which corresponds to an intermediate case between open and closed boundary conditions.

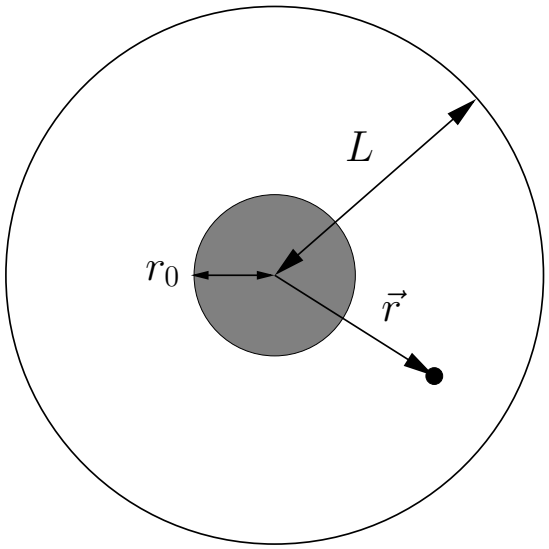

Figure 3.1: Schematic of the system under investigation, consisting of a circular membrane of radius L with a circular inclusion of radius r_0 at the center. The membrane is supported by a flat surface to which it is attached by a single adhesion bond located at $\vec{r}$. (Adapted from [54])

The integral in eq. 3.1 has been evaluated numerically for different values of r_0 and L, and for $r_0 < |\vec{r}| < L$. Our calculations reveal that the attachment free energy is very well approximated by the following expression

$$F(\vec{r}, r_0, L) \sim 2k_BT \ln \frac{(|\vec{r}| - r_0)}{l} + nk_BT \ln \frac{(L - |\vec{r}|)}{l} + C(r_o, L), \tag{3.2}$$

with $n = 1$ for an open outer boundary, and $n = 2$ for a closed boundary. Introducing the dimensionless distance $0 < x = (|\vec{r}| - r_0)/(L - r_0) < 1$, eq. 3.2 can be also expressed as

$$F(x) \equiv F(\vec{r}, r_0, L) - \ln \left(\frac{L - r_0}{l} \right)^{2+n} - C(r_o, L) \sim 2k_BT \ln(x) + nk_BT \ln(1 - x). \tag{3.3}$$

Our numerical results along with eq. 3.3 are plotted in figs. 3.2(A) and 3.2(B) for an

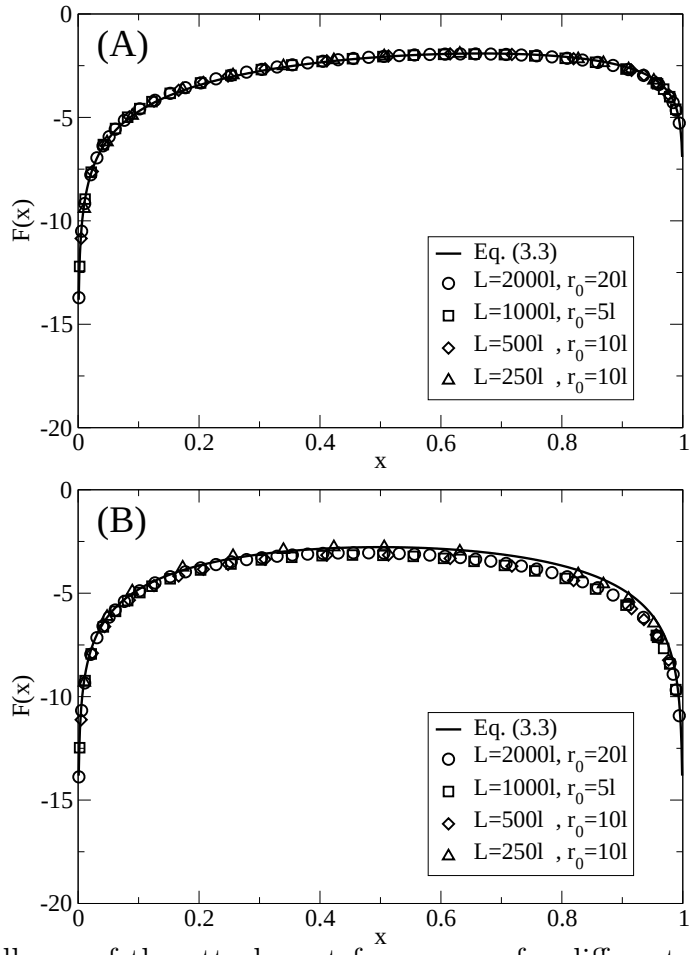

Figure 3.2: Data collapse of the attachment free energy for different values of $|\vec{r}|$, r_0, and L, as a function of the dimensionless distance $x = (|\vec{r}| - r_0)/(L - r_0)$. The data in (A) and (B) corresponds to systems with open and closed outer boundaries, respectively. (Adapted from [54])

open and closed boundary, respectively. When the adhesion bond is located far away from the outer boundary, i.e. for $x \ll 1$, the attachment free energy is dominated by the first term $F \simeq 2k_BT\ln(x)$, which has been previously derived as the pair potential of mean force between two adhesion bonds [42]. In the vicinity of an outer closed boundary ($x \lesssim 1$), one gets $F \simeq 2k_BT\ln(1-x)$, which implies that the adhesion bond is attracted to the nearest point on the outer closed boundary as if this point is another adhesion bond. For an open boundary, the prefactor of the second term in eq. 3.3 is reduced by half from $n = 2$ to $n = 1$. This can be rationalized by noticing that an open boundary is identical to the midplane between two adhesion bonds in a twice larger system. The pair potential between

the adhesion bond and its image is $2k_BT\ln[2(1-x)] = 2k_BT\ln[(1-x)] + C$, and this energy is equally divided between the real and imaginary halves of the system.

How strong is the attraction between the adhesion bond and the inner inclusion? From eq. 3.2 we find that the probability distribution function $P(\vec{r}) \sim \exp\left[-F(\vec{r}, r_0, L)/k_BT\right]$ of the adhesion bond is given by

$$P(\vec{r}) = \frac{1}{Z}\frac{1}{(|\vec{r}| - r_0)^2(L - |\vec{r}|)^n}, \tag{3.4}$$

where the normalization factor is

$$Z = \int_{r_0+l}^{L-l} \frac{2\pi r dr}{(r - r_0)^2(L - r)^n}. \tag{3.5}$$

In the case of an open outer boundary ($n = 1$), the mean distance between the adhesion bond and the surface of the inner inclusion is given by

$$\langle r\rangle - r_0 \equiv \Delta = \frac{(L^2 - r_0^2)\ln\left(\frac{L-r_0-l}{l}\right)}{2L\ln\left(\frac{L-r_0-l}{l}\right) + r_0(r_0 - L)\left[\frac{2l+r_0-L}{l(L-r_0-l)}\right]}, \tag{3.6}$$

which for $L \gg r \equiv |\vec{r}| \gg r_0$, simplifies to $\Delta \sim L/2$. The fact that the mean separation Δ grows linearly with the size of the membrane may be considered as an indication that the adhesion bond is not bound to the inclusion. However, a closer inspection of eq. 3.4 reveals that the adhesion bond spends most of its time near the boundary of the inner inclusion. To quantify this phenomenon, we introduce the length scale Δ^*, which is the width of the shell around the inner inclusion where the probability to find the adhesion bond is 0.5. The length Δ^* is determined by solving the equation

$$P_{\rm acc}(\Delta^*) = \int_{r_0+l}^{r_0+\Delta^*} 2\pi|\vec{r}|P(|\vec{r}|)dr = \frac{2L\ln\left(\frac{\Delta^*}{l}\right) + r_0(r_0 - L)\left(\frac{l-\Delta^*}{l\Delta^*}\right)}{2L\ln\left(\frac{L-r_0-l}{l}\right) + r_0(r_0 - L)\left[\frac{2l+r_0-L}{l(L-r_0-l)}\right]} = 0.5. \tag{3.7}$$

Our results for Δ^* are plotted in fig. 3.3 as a function of r_0 and for $L \gg r_0$. The results

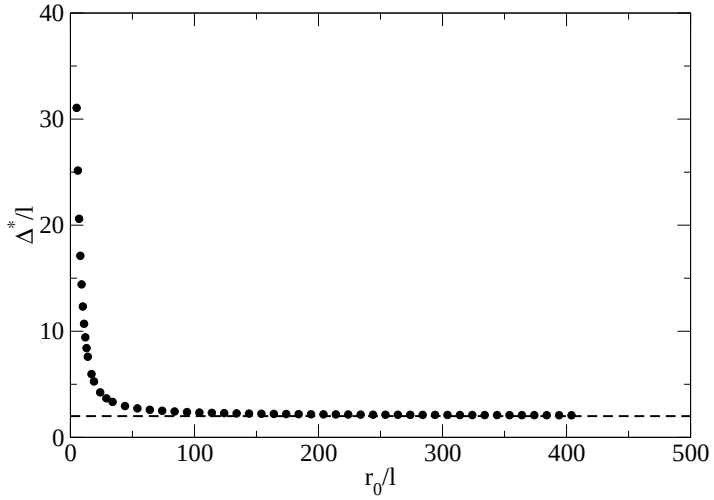

Figure 3.3: The width Δ^* of the shell around the inclusion, as a function of the radius of the inclusion r_0. The dashed horizontal line corresponds to the solution of eq. 3.7, $\Delta^* = 2l$, for asymptotically large r_0. (Adapted from [54])

shows that Δ^* is a monotonically decreasing function of r_0. For very small inclusions of size $r_0 \sim l$, the length $\Delta^* \gg l$. This result is consistent with the observation of ref. [42] that the fluctuation-mediated pair potential is too weak to bind two adhesion bonds to each other. For inclusions of size $r_0 \gtrsim 20l$, the length $\Delta^* < 5l$; and for asymptotically large inclusions ($r_0 \to \infty$), $\Delta^* \to 2l$. In other words, although $\Delta \sim L/2$, the adhesion bond is likely to be found within a thin shell around the surface of a sufficiently large inclusion.

For a closed outer boundary, the radial distribution function of the adhesion bond

$$g(r) \equiv 2\pi r P(|\vec{r}|) = \frac{r}{(r-r_0)^2(L-r)^2} \left\{ \frac{(L-r_0)^3}{(L+r_0)\left[2\ln\left(\frac{L-r_0-l}{l}\right) + (r_0-L)\left(\frac{2l+r_0-L}{l(L-r_0-l)}\right)\right]} \right\}. \tag{3.8}$$

(The expression appearing in braces in eq. 3.8 is a normalization constant that depends on r_0 and L). The radial distribution function $g(r)$, which is plotted in fig. 3.4 for $r_0 = 4l$ and $L = 100L$, increases rapidly as one approaches both the inner and outer boundaries of the membrane. However, unlike the probability density per unit area $P(\vec{r})$ which is symmetric with respect to the mid-radius $r_m = (L + r_0)/2$, the radial distribution function

$g(r) \sim rP(|\vec{r}|)$ is much higher near the outer boundary than the inner one. This, of course, is directly related to the fact that there is simply more membrane area near the outer boundary. In the example plotted in fig. 3.4 ($r_0 = 4l$, $L = 100l$), the probabilities to find the adhesion bond within a shell of size $4l$ around the outer and inner boundaries are 72.5% and 4.5%, respectively. For a bigger membrane of size $L = 1000l$ (which, assuming that l is of the order of a few nanometers, is a reasonable estimate for the size of the cell plasma membrane), these probabilities change to 79% and 0.5%, respectively. These numbers suggest that the adhesion bond is likely to be "adsorbed" at the outer boundary. This, however, is only part of the story. If the adhesion bond is located near the inner boundary, it is not going to easily escape to the outer rim. The inset on fig. 3.4 shows the effective free energy $F_g(r) \equiv -k_B T \ln [g(r)]$, exhibiting a free energy barrier of $\sim 4k_B T$ that blocks the migration of the adhesion bond from the inner boundary to the outer one. The barrier on the opposite direction is of $\sim 7k_B T$. For $L = 1000l$, the free energy barriers increase to $\sim 7k_B T$ and $\sim 12k_B T$ for the escape from the inner and outer boundaries, respectively. Thus, as in the case with an open boundary discussed above, an adhesion bond located near the inner boundary is likely to stay there for relatively long times.

3.2 Distribution of adhesion bonds around an inclusion

The previous section dealt with the localization of a single adhesion bond near the boundaries of the system. Cellular adhesion, however, involves an ensemble of adhesion bonds which may cluster into adhesion domains. In chapter 2, we demonstrated that the formation of adhesion domains occur only when, *in addition to the fluctuation-induced attraction*, there is also a direct attractive potential between the adhesion bonds. Here, we wish to understand whether this picture is changed by the presence of a membrane inclusion that serve as a potential nucleation seed for an adhesion domain. One can envision a scenario where a thin shell of adhesion bonds is formed around the inclusion, effectively increasing its size and

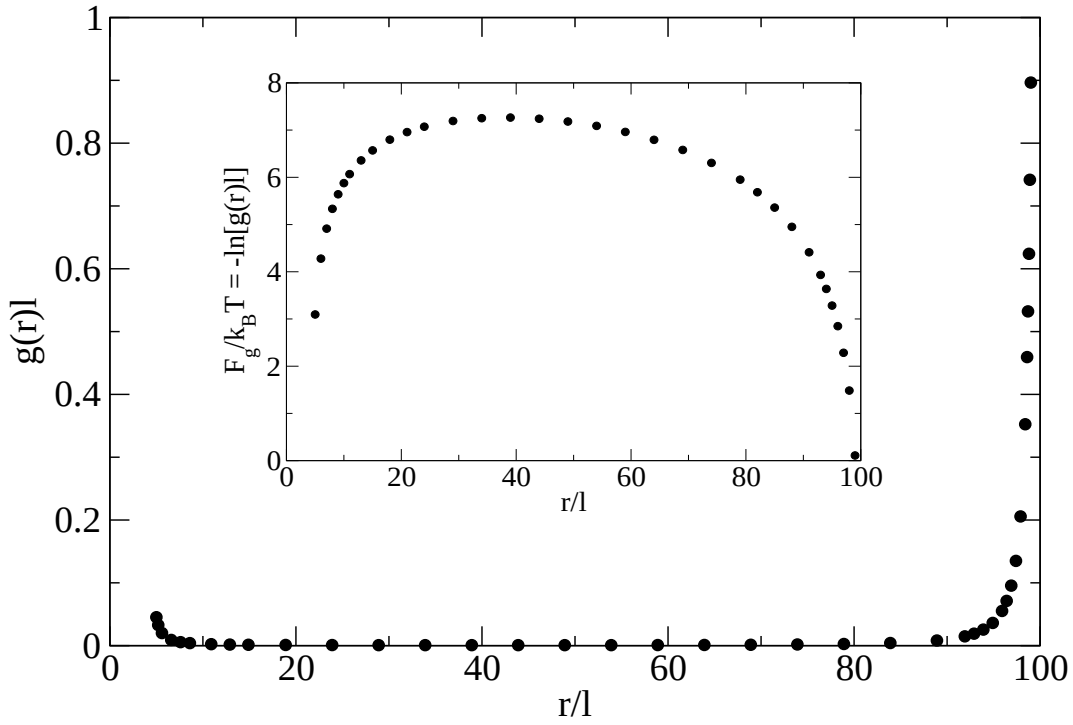

Figure 3.4: The radial distribution function g as a function of r, for $r_0 = 4l$ and $L = 100l$. The inset shows the corresponding free energy, $F_g = -k_B T \ln[g(r)l]$. (Adapted from [54])

promoting the recruitment of more adhesion bonds. The opposite scenario, in which the addition of adhesion bonds self-screen the attraction towards the inclusion, is also plausible. In order to investigate this issue, we performed MC simulations of the lattice model defined by the same means as in chapter 2, with $\epsilon = 0$ (i.e., with fluctuation-induced interactions only and without an additional direct attraction). We simulated circular systems with $r_0 = 4l$ and $L = 100l$ (where l is the lattice spacing), with both open and closed boundary conditions. Our simulations were conducted at relatively low concentrations of adhesion bonds, $\phi = 0.01$ and $\phi = 0.05$.

We measured the number density (per unit area) of adhesion bonds as a function of $\vec{r}$. To allow comparison with the probability distribution $P(\vec{r})$ (eq. 3.4), we normalized the number density to the total number of adhesion bonds. Our results for the normalized number density, $\rho(\vec{r})$, are depicted in fig. 3.5(A) and 3.5(B) for open and closed boundaries, respectively. Both figures demonstrate that the fluctuation-induced attraction to the boundaries

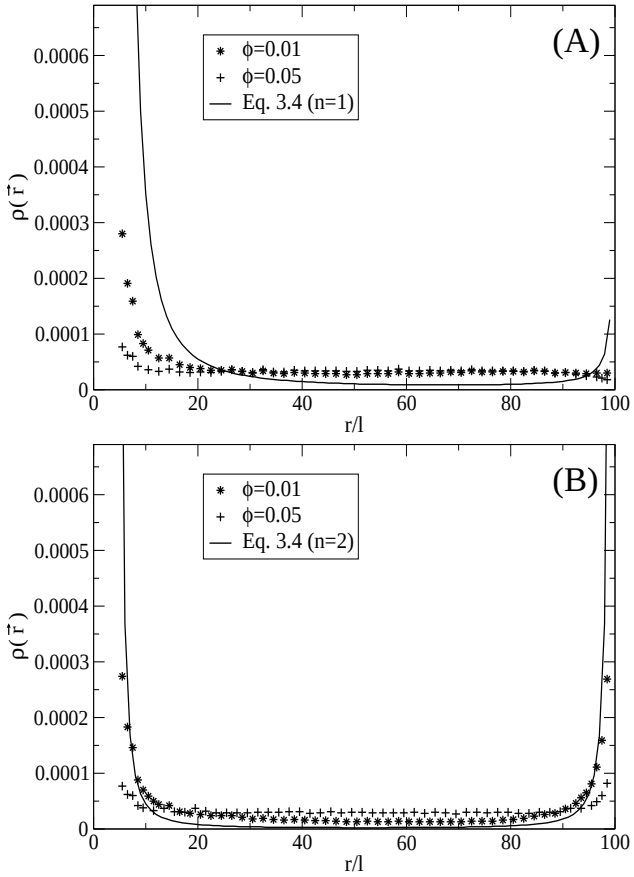

Figure 3.5: The normalized number density $\rho(\vec{r})$ as a function of $r = |\vec{r}|$. Data shown in the figure corresponds to $r_0 = 4l$ and $L = 100l$, for systems with (A) open and (B) closed outer boundaries. The solid lines depict the probability distribution of a single adhesion bond. (Adapted from [54])

is self-screened by the presence of adhesion bonds. Comparison of our results for $\phi = 0.01$ (depicted by stars in both figures) and $\phi = 0.05$ (pluses), with eq. 3.4 for a single adhesion bond (solid lines), reveals that the self-screening effect is increased with the increase in the concentration ϕ. For an open boundary, the slight increase in $P(\vec{r})$ near the outer boundary disappears already at $\phi = 0.01$. For $\phi = 0.05$, the density $\rho(\vec{r})$ is almost constant with no significant affinity of adhesion bonds towards the inner boundary. The same trends are also observed in the case of a closed boundary, where $P(\vec{r})$ increases very sharply near both boundaries. When the concentration ϕ increases, these maxima are quickly lowered, and the number density $\rho(\vec{r})$ becomes almost uniform.

3.3 Summary

In this chapter we continued our investigation of the entropic, fluctuation-induced, attraction between adhesion bonds in supported biological membranes. The focus here was on the possible role played by the membrane boundaries as nucleation seeds for the formation of adhesion domains. Residence of adhesion bonds near the cell boundaries is thermodynamically favorable because it lowers the entropic cost associated with the suppression of the membrane thermal fluctuations around the adhesion bonds. We started our investigation by looking at the pair interaction between an adhesion bond and a circular membrane inclusion, and calculating the distribution function of the adhesion bond around the inclusion. In the case of an open outer cell boundary, the probability density of the adhesion bond decays algebraically with the distance from the surface of the inclusion. Although the mean pair distance grows linearly with the size of the membrane, the distribution function is such that the adhesion bond spends most of its time in the immediate vicinity of the inclusion. When the outer membrane boundary is closed, the probability distribution per unit area is symmetric with respect to the mid radius. In this case, the adhesion bond is likely to be found near the outer boundary, which is much larger than the inner one. Diffusion of the adhesion bonds between the two boundaries is limited by the existence of a substantial free energy barrier in the middle of the membrane.

Does this analysis imply that the cell boundaries can serve as nucleation seeds for adhesion domains? Perhaps yes, but probably not due to the fluctuation-induced mechanism alone. Our simulation results show that even at small densities of adhesion bonds, the entropic attraction towards the cell boundaries are entirely self-screened. This observation is consistent with our previous study of a lattice-gas model of adhesion bonds, where it has been found that the fluctuation-induced interactions are not sufficient to allow the formation of adhesion domains.

Chapter 4

Discussion

Understanding the thermodynamics of adhesion processes and the molecular interactions involved in cell adhesion are important topics in biological and biophysics, with implications for a variety of cellular processes. It is also critical for the development of drug delivery systems which are based on liposome-target cell adhesion. While a random distribution of adhesion bonds produce only weak attachment between membranes, the aggregation of the adhesion bonds into domains cause a much stronger adhesive binding. The formation of these domains is facilitated by a variety of biomolecular interactions (e.g., hydrophobic and van der Waals interactions), as well as through two membrane-induced mechanisms. The first mechanism is the Casimir-like attraction between two bonds, which originates from the reduction in the amplitude of the membrane thermal fluctuations in the vicinity of the bonds and the associated entropy loss. The resulting increase in the free energy of the membrane is minimized when the two bonds come within close proximity of each other, in which case the area where the thermal fluctuations are suppressed is reduced. The second mechanism is related to the tendency of new bonds to form next to existing ones [57]. This "binding cooperativity" effect stems from the fact that the ligand-receptor binding probability is highest when the separation between the ligand and the receptor on the opposite surfaces is close to the bond length - conditions which are likely to occur near already existing bonds [32].

In addition, since the formation of new bonds leads to an overall reduction in the membrane roughness, it also increases the binding probability and assists the formation of even more bonds. Generally speaking, the first mechanism is likely to contribute to the aggregation of irreversible bonds with large binding energies, while the second one is probably relevant to the formation of metastable domains of weaker reversible bonds.

In this thesis, we examined the first mechanism of Casimir-like fluctuation-induced attraction, and investigated its contribution to the aggregation of adhesion domains. We derived the non-additive many-body potential of mean-force between adhesion bonds, and used it within a 2D lattice-gas model for adhesion bonds. The lattice-gas model allowed us to extract the phase diagram of the system. Using mean field theory and MC computer simulations, we showed that the fluctuation-induced interactions alone are too weak to induce domain formation. They do, however, greatly reduce (to below the thermal energy k_BT) the strength of the direct interactions at which the transition takes place.

In addition, we studied the formation of adhesion domains in cellular membranes which also include trans-membrane proteins that, as the adhesion bonds, reduce the amplitude of the membrane thermal fluctuations. We examined if the existence of an inclusion on the membrane surface can change the phase behavior of adhesion bonds. We found that, in the case of single adhesion bond and inclusion, the adhesion bond has high probability to be found in the vicinity of the inclusion. In the case of many adhesion bonds, the affinity towards the inclusion is self-screened by the adhesion bonds, and felt only by the bonds residing near the surface of the inclusion. This result is consistence with our conclusions that the fluctuation-induced interactions are too week to induce domain formation. Without additional attractive direct interactions, the problem of aggregation of adhesion bonds near a membrane inclusion is similar to the problem of gas to liquid condensation, in which the inclusion is analogous to a nucleation seed. Introducing the nucleation seed into such a system without reducing the temperature to below criticality, is not going to drive the system into the condensed phase.

Our studies can be extended in several directions. First, our analysis was based on the

assumption that the adhesion bonds attach the membrane directly to the supporting surface. In reality, the bond has a finite length which may fluctuate and, therefore, the bonds should be modeled as elastic springs. Second, adding different ligand-receptor bonds with different bond length to the system can cause, due to the length mismatch, the segregation of the adhesion bonds [45]. Third, we also need to consider the case of reversible ligand-receptor bonds and the associated "binding cooperativity" effect. This effect can be studied via kinetic MC simulations. Fourth, we can also add additional energy contributions to the model Hamiltonian, such as a surface tension term and other external potentials. These additional contributions change the membrane fluctuations spectrum. It will be especially interesting to examine the case where the external potential causes attraction of the membrane at a height which is different then the bond height. In this case, we expect a competition between specific and non-specific binding. Finally, we also leave for a future work the problem of domain formation in membranes with several inclusions.

Bibliography

[1] R. Lipowsky, E. Sackmann (Eds.), *Handbook of Biological Physics: Structure and Dynamics of Membranes* (Elsevier, Amsterdam, 1995).

[2] B. Alberts, D. Bray, J. Lewis, M. Raff, K. Roberts, J. D. Watson, *Molecular Biology of the Cell* (Garland, New York, 1994).

[3] S. A. Safran, *Statistical Thermodynamics of Surfaces, Interfaces, and Membranes Addison* (Wesley, New York, 1994).

[4] R. B. Gennis, *Biomembranes: Molecular Structure and Function*, (Springer, New York, 1989).

[5] T. Salditt, J. Phys.: Condens. Matter **17**, R287 (2005).

[6] M. Tanaka, E. Sackmann, Nature **437**, 656 (2005).

[7] H. A. Rinia, G. W. H. Wurpel, M. Müller, *Visualization and characterization of domains in model membranes, in:* A. Ottova-Tien (Ed.), *Advances in Planar Lipid Bilayers and Liposomes* (Elsevier, Amsterdam, 2006).

[8] M. Tanaka, E. Sackmann, Phys. Stat. Sol. (a) **203**, 3452 (2006).

[9] P. P. Girard, E. A. Cavalcanti-Adam, R. Kemkemer, J. P. Spatz, Soft Matter **3**, 307 (2007).

[10] J. Salafsky, J. T. Groves, S. G. Boxer, Biochemistry **35** 14773 (1996).

[11] E. Sackmann, Science **271**, 43 (1996).

[12] Kloboucek, A. Behirsch, J. Faix, E. Sackmann, Biophys. J. **77**, 2311 (1999).

[13] Y. Kaizuka, T. J. Groves, Biophys. J. **86**, 905 (2004).

[14] A.-S. Smith, B. G. Lorz, U. Seifert, E. Sackmann, Biophys. J. **90**, 1064 (2006).

[15] A. Ananthakrishnan, A. Ehrlicher, Int. J. Biol. Sci. **3**, 303 (2007).

[16] E. Lindahl, O. Edholm, Biophys J **79**, 426 (2000).

[17] M. Müller, K. katsov, M. Schick, J. Polym. Sci. B: Polym. Phys **41**, 1441 (2003).

[18] O. Farago, J. Chem. Phys. **119**, 596 (2003).

[19] J. C. Shillcock, R. Lipowsky, J. Chem. Phys. **117**, 5048 (2002).

[20] R. D. Groot, K. L. Rabone, Biophys. J. **81**, 725 (2001).

[21] R. D. Groot, P. B. Warren, J. Chem. Phys. **107**, 4423 (1997).

[22] J. Fraaije, J. Chem. Phys. **99**, 9202 (1993).

[23] E. Helfand, Y. Tagami, J. Chem. Phys. **56**, 3592 (1972).

[24] J. M. Drouffe, A. C. Maggs, and S. Leibler, Science **254**, 1353 (1991).

[25] H. Noguchi and M. Takasu, Phys. Rev. E **64**, 041913 (2001); H. Noguuchi, J. Chem. Phys. **117**, 8130 (2002).

[26] G. La Penna, S. Letardi, V. Minicozzi, S. Morante, G. C. Rossi, and G. Salina, Eur. Phys. J. E **5**, 259 (2001).

[27] G. Gompper and M. Schick, "Self-assembling amphiphilic systems," in *Phase Transitions and Critical Phenomena*, edited by C. Domb and J. L. Lebowitz (Academic, London, 1994).

[28] W. Helfrich, Z. Naturforsch. **28C**, 693 (1973).

[29] D. H. boal, *Mechanics of the cell* (Cambridge University Press, Cambridge, 2002).

[30] D. A. Lauffenburger and J. Linderman, *Receptors: Models for binding, Trafficking, and Signaling* (Oxford University Press, Oxford, 1995).

[31] A.-S. Smith and U. Seifert, Soft Matter **3**, 275 (2007).

[32] T. R. Weikl, M. Asfaw, H. Krobath, B. Różycki and R. Lipowsky, Soft Matter **5**, 3213 (2009).

[33] V. Naggli, Int. J. Biochem. Biochem Cell Biol. **35**, 1619 (2003).

[34] T. M. Allen and P. R. Cullis, Science **303**, 1818 (2004).

[35] K. Giehl and A. Menke, Front. Biosci. **13**, 3975 (2008).

[36] B. Geiger, A. Bershadsky, R. Pankov, and K.M. Yamada, Nat. Rev. Mol. Cell Biol. **2**, 793 (2001).

[37] J. Israelachvili, *Intermolecular and Surface Forces* (Academic Press, London, 1985).

[38] B. Simon, *The Statistical Mechanics of Lattice Gases I* (Princeton University Press, Princeton, 1993).

[39] J. Braun, J. R. Abney, and J. C. Owicki, Nature **310**, 316 (1984).

[40] O. Farago, Arxiv: cond-mat/1107.5126 (2011).

[41] O. Farago, Phys. Rev. E **78**, 051919 (2008).

[42] O. Farago, Phys. Rev. E **81**, 050902(R) (2010).

[43] R. Bruinsma, M. Goulian, P. Pincus, Biophys. J **67**, 746 (1994).

[44] W . Helfrich, Z Naturforsch C. **33A**, 305 (1978).

[45] T.R. Weikl, R. Lipowsky, *in Advances in Planar Lipid Bi-layers and Liposomes*, edited by A.L. Liu, Vol. 5 (Elsevier, Amsterdam, 2007).

[46] T. Speck, Phys. Rev. E **83**, 050901(R) (2001).

[47] N. Weil and O. Farago, Eur. Phys. J. E **33**, 81 (2010).

[48] R. Parthasarathy and J. T. Groves, J. Phys. Chem. B **110** (16), 8513 (2006).

[49] N. Taulier, M. Waks, T. Gulik-Krzywicki, and W. Urbach, Europhys. Lett. **59** (1), 142 (2002).

[50] R. Bruinsma and P. Pincus, Curr. Opin. Solid State Mater. Sci. **1** ,401 (1996).

[51] J.-M. Park and T. C. Lubensky, J. Phys. I **6**, 1217 (1996).

[52] M. Kardar and R. Golestanian, Rev.Mod. Phys. **71**, 1233 (1999).

[53] K. S. Kim, J. Neu, and G. Oster, Phys. Rev. E **61** (4), 4281 (2000).

[54] N. Weil and O. Farago, submitted to Phys. Rev. E (2011).

[55] B. Różycki, R. Lipowsky, and T. R. Weikl, New J. Phys. **12**, 095003 (2010).

[56] N. J. Burroughs1, K. K¨hler, V. Miloserdov, M. L. Dustin, P. A. van der Merwe, and D. M. Davis, Plos. Comut. Biol. **7**, e1002076 (2011).

[57] E. Reister, T. Bihr, U. Seifert, and A. S. Smith, New J. Hpys. **13**, 025003 (2011).